Plasma Dispersion Relation Measurements through Active Injection of Wave Packets

IEPC-2019-A623

Presented at the 36th International Electric Propulsion Conference
University of Vienna, Austria
September 15-20, 2019

Sebastián Rojas Mata* and Edgar Y. Choueiri†
Electric Propulsion and Plasma Dynamics Lab, Princeton University, Princeton, NJ, 08544, USA

A probe-based diagnostic is developed to emit and receive harmonically-rich wave packets in a plasma for measuring the dispersion relation simultaneously at multiple frequencies. The underlying methodology allows for expedited data acquisition and gives direct control over the signal-to-noise ratio of the measurements. The dispersion relation is measured by conducting a frequency-domain analysis of ion-saturation-current probe time-traces that uses coherence metrics to identify wave propagation and interferometry to calculate wavenumber as a function of frequency. The diagnostic is implemented in a 250 W magnetized RF argon plasma source to measure the dispersion relation of electrostatic ion-cyclotron waves perpendicular to the background magnetic field. A comb generating circuit excites harmonically-rich wave packets by generating tens of harmonics of an input square wave's fundamental frequency. The nearly three dozen simultaneously measured wavenumbers agree with the prediction of a fluid plasma wave model for frequencies spanning 6 harmonics of the ion-cyclotron frequency.

Nomenclature

ω	Angular frequency, rad/s
f	Linear frequency, Hz
k	Wavenumber, rad/m
p	Plasma parameter
n	Density, m^{-3}
T	Temperature, eV
B	Magnetic field, G
v	Velocity, m/s
m	Mass, kg
d	Distance, m
$\mathfrak{I}$	Current, A
V_{in}	Wave driving signal, V
λ_D	Debye length, m
ρ	Larmor radius, m
v_{th}	Thermal velocity, m/s
v_d	Drift velocity, m/s
v_{ph}	Phase velocity, m/s
v_g	Group velocity, m/s
c_S	Ion sound speed, m/s
c	Speed of light, m/s
I_n	n^{th} order modified Bessel function of the first kind
Z	Plasma dispersion function of Fried and Conte
$\mathcal{F}_W$	Windowed discrete Fourier transform
$\hat{a}$	Fourier image of quantity a
a^*	Complex conjugate of quantity a

Subscript

e	Electron
i	Ion
o	Neutral
s	Species
p	Plasma
c	Cyclotron

*Graduate Student, MAE Department
†Chief Scientist, EPPDyL, Professor, Applied Physics Group, MAE Department

I. Introduction

In many plasma propulsion applications, the measurement of the dispersion relation is needed to identify plasma wave modes which may affect physical processes, such as particle transport,[1–4] or grow into instabilities that modify the discharge.[5,6] In theoretical analyses, the dispersion relation is often needed to provide some of the input for plasma transport models like quasilinear theory.[7,8] The dispersion relation of a plasma is typically written as

$$\mathcal{D}(\omega, \mathbf{k}; p_1, p_2, \dots) = 0, \tag{1}$$

where $\mathcal{D}$ is a function relating the wave frequency ω and the wavenumber vector $\mathbf{k}$ to plasma parameters p_i such as electron density or background magnetic field. Solving Eq. 1 for its complex roots gives a relationship between ω and $\mathbf{k}$. Numerical characterization tools[9] can provide information about the relevant wave modes present in a thruster configuration by numerically solving for the zeros of a particular dispersion relation in $(\omega, \mathbf{k})$-space given a set of input plasma parameters. However, the assumptions behind the derivation of the dispersion relation may limit the accuracy of the numerical results, as the chosen plasma models might not include all the relevant physics. Therefore, numerical investigations require additional experimental validation to verify their accuracy. Two such existing methods for measuring the dispersion relation are passive probe interferometry[10] and laser induced fluorescence (LIF).[11,12]

Passive probe interferometry relies on the cross-correlation of the time-dependent voltage or current traces of two physical probes immersed in a plasma at known locations. Since the distance between the probes is known, determining the phase difference between the two probe signals yields a measurement of the dispersion relation. However, like any probe, passive probe interferometry is intrusive and may alter the plasma probed. Additionally, noisy plasma environments can overwhelm the signal of wave modes of interest, resulting in low signal-to-noise ratio (SNR) measurements which require statistical methods to extract meaningful information.[4,13]

Alternatively, the non-intrusive LIF technique shines the beam of a tunable laser through the plasma, sweeping over a range of wavelengths in which the plasma's ions can be excited to metastable atomic states. Measuring the induced fluorescence from the subsequent spontaneous relaxation of the ions provides measurements of the background and first-order perturbed ion velocity distribution functions. Data fits to solutions of the perturbed ion Vlasov equation provide a measurement of the dispersion relation.[11,12] While attractive for its non-intrusive nature, the LIF technique involves costly equipment and two optical lines-of-sight access points to the plasma volume. Due to its reliance on fluorescence, it is incompatible with certain gases, and a given laser is compatible with one gas only.

Both methods attempt to 'listen' to collective modes that are naturally excited in the plasma. These modes are generally already in the saturation stage, which obscures their linear growth stage. On the other hand, an active technique that relies on 'ringing' the plasma has the advantage of capturing both the phase and growth components of the linear dispersion relation.[14–17] In this paper we present an active diagnostic which emits harmonically-rich wave packets instead of the single wave injection technique from previous work. This active injection of wave packets has the advantage of measuring the linear dispersion relation simultaneously at multiple frequencies.

We structure the paper as follows. In Section II we overview the active wave packet injection (AWPI) concept and the frequency-domain analysis to interpret experimental data. Section III presents the AWPI diagnostic we developed for use in an experimental study in a magnetized RF argon plasma source. The theory of the expected electrostatic ion-cyclotron waves is described in Section IV. We present measurements in Section V of the dispersion relation, ending with concluding remarks in Section VI.

II. Active Wave Packet Injection Methodolgy

Active wave injection systems generally consist of an emitter probe or antenna along with two or more receiver ion-saturation-current probes. In Fig. 1 we show an example system with an antenna and two receiver probes immersed in the plasma. The system can be generalized to contain more receiver probes, so that each pair of receiver probes measures the wavenumber along the direction parallel to the line joining them. A time-dependent voltage signal $V_{in}(t)$ sent to the antenna excites an electrostatic plasma wave, with compressions and rarefactions of plasma density passing by the receiver probes located downstream. This allows targeting the expected frequency range (e.g. from theory) of the plasma wave mode in question. Analysis of the current traces $\mathcal{I}_1(t)$ and $\mathcal{I}_2(t)$ provides information about the wavenumber $\mathbf{k}$ as a function

of the wave frequency ω. Though previous work used sinusoidal excitations and our AWPI methodology uses harmonically-rich excitations, the frequency-domain analysis to measure the dispersion relation we use is applicable to both. To identify coherent wave propagation over background random noise in the signals recorded, we compute spectrum and correlation estimates of the digitally recorded $\mathcal{I}_1(t_n)$ and $\mathcal{I}_2(t_n)$. We follow a nonparametric signal processing procedure that uses Welch's method[18] to produce estimates of auto- and crosspower spectra as well as an estimate of the coherence spectrum of the two probe signals.[10,19,20]

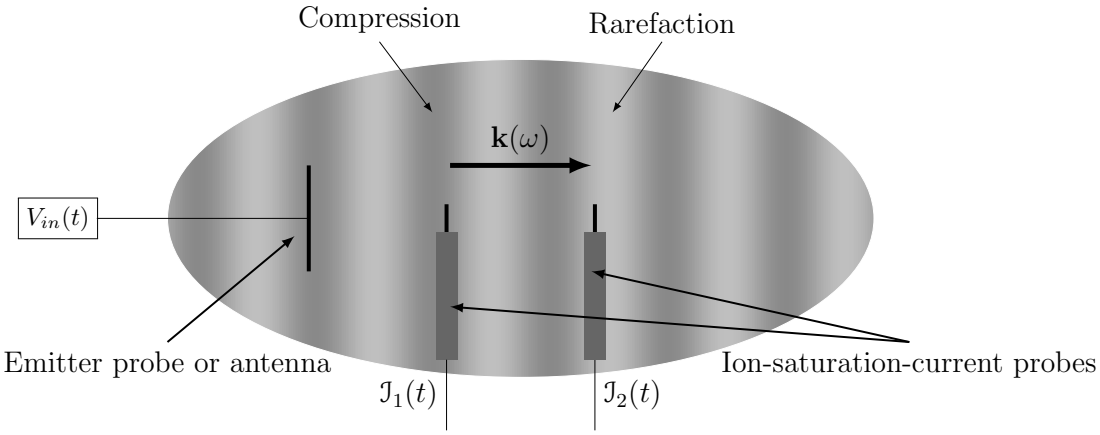

Figure 1. Active wave injection concept. The antenna excites traveling compressions and rarefactions of plasma density which result in time-dependent ion-saturation-current traces recorded by the receiver probes downstream. The AWPI concept extends this to use harmonically-rich wave packets instead of sinusoidal excitations.

Assume the recorded current traces $\mathcal{I}_1(t_n)$ and $\mathcal{I}_2(t_n)$ are of length N points. We divide each into S equal data segments of length M points, giving the sets $\{\mathcal{I}_{1,1}, \mathcal{I}_{1,2}, \ldots, \mathcal{I}_{1,j}\}$ and $\{\mathcal{I}_{2,1}, \mathcal{I}_{2,2}, \ldots, \mathcal{I}_{2,j}\}$, $j \in [1, S]$. We overlap the successive data segments by 50%, so that, for example, the second half of the first data segment is also the first half of the second data segment. This is a common recommendation when applying Welch's method to decrease random error and not sacrifice too much of the frequency resolution of the spectra.[19,20] We then take a windowed discrete Fourier transform of each data segment,

$$\hat{\mathcal{I}}_{1,j}(f_n) = \mathcal{F}_{\mathcal{W}}\{\mathcal{I}_{1,j}(t_n)\}, \quad \hat{\mathcal{I}}_{2,j}(f_n) = \mathcal{F}_{\mathcal{W}}\{\mathcal{I}_{2,j}(t_n)\}. \tag{2}$$

We use a Hanning window "since it provides a good compromise between amplitude accuracy and frequency resolution (Ref. 20)." We calculate the autopower spectra of the current traces $\mathcal{I}_1$ and $\mathcal{I}_2$ by averaging over the autopower spectra of the data segments, so that

$$P_{11}(f_n) = \frac{A}{S}\sum_{j=1}^{S} \hat{\mathcal{I}}^*_{1,j}(f_n)\hat{\mathcal{I}}_{1,j}(f_n) \quad \text{and} \quad P_{22}(f_n) = \frac{A}{S}\sum_{j=1}^{S} \hat{\mathcal{I}}^*_{2,j}(f_n)\hat{\mathcal{I}}_{2,j}(f_n), \tag{3}$$

where

$$A = \frac{1}{M^2 P_W^2}, \quad P_W = |\mathcal{F}_W\{1\}| \tag{4}$$

is an amplitude correction factor to account for the power of the window. Similarly, we compute the crosspower spectrum

$$P_{12}(f_n) = \frac{A}{S}\sum_{j=1}^{S} \hat{\mathcal{I}}^*_{1,j}(f_n)\,\hat{\mathcal{I}}_{2,j}(f_n) \tag{5}$$

and a normalized version of it called the coherence spectrum

$$\gamma_{12}(f_n) = \frac{P_{12}(f_n)}{\left[P_{11}(f_n)P_{22}(f_n)\right]^{1/2}}, \tag{6}$$

both of which provide information about correlated signals present in the probes. Specifically, the magnitude of the coherence spectrum measures how linearly related the two probe signals are, with $|\gamma_{12}| = 0$ denoting no relation and $|\gamma_{12}| = 1$ denoting a complete linear relation. We consider wave propagation to be coherent when $|\gamma_{12}| > 0.95$ and the uncertainty is less than 0.05.

The real wavenumber spectrum of coherently propagating waves is

$$k_r(f_n) = \frac{\text{Arg}\{P_{12}(f_n)\}}{d_{12}}, \tag{7}$$

where d_{12} is the distance between the two receiver probes. The imaginary wavenumber spectrum, which represents spatial growth or decay, is calculated from

$$k_i(f_n) = -\frac{1}{2}\log\left[\frac{P_{22}(f_n)}{P_{11}(f_n)}\right]. \tag{8}$$

The phase and group velocities,

$$v_{ph} = \frac{\omega}{k_r} \quad \text{and} \quad v_g = \frac{d\omega}{dk_r}, \tag{9}$$

can then be calculated.

III. Experimental Investigation

A. AWPI Diagnostic

A schematic of the AWPI diagnostic is depicted in Fig. 2 and a photograph in Fig. 3. Two 1.5 cm by 5 cm, 0.51 mm thick molybdenum plates resting on alumina stand-offs which attach to a 1.27 cm diameter G-10 tube consitute the antenna. We choose this antenna geometry as previous investigations used it to excite electrostatic modes.[15,17] Tungsten wires attach each plate to coaxial cables which connect the antenna back to a harmonic comb generating circuit (see below). The diagnostic has three receiver probes to measure wavenumbers in the directions parallel and perpendicular to the antenna blades. The perpendicular tips are 0.1 cm apart and the parallel tip is 0.5 cm away, all sitting ∼1 cm away from the antenna. The probe tips, which are biased to -27 V, are 2 mm long, 0.254 mm thick tungsten wires housed inside alumina tubes cased in copper tubes for capacitive shielding and glass tubes for protection from the plasma environment. The tungsten wires connect to coaxial cables which carry the signals to the data acquisition system. The full electrical diagram for the antenna, probe, and data acquisition circuits is in Appendix A.

B. Harmonic Comb Generating Circuit

We base the design of our harmonic comb generating circuit on previous work that sought a size, weight, and power-constrained solution to *in-situ* diagnosing of wireless devices.[21] As shown in Fig. 4a, the circuit contains a square wave signal generator, a high-pass filter, and a diode, the latter two of which are depicted in Fig. 4b. The square wave contains only odd-integer harmonics of its fundamental frequency, which decrease in amplitude inversely proportional to harmonic number. The high-pass filter acts as a differentiator and attenuates the lower-frequency harmonics of the square wave to decrease the disparity between amplitudes (i.e. it accentuates the sharp edges of the square wave). The directional nature of the diode breaks the positive-negative symmetry of the signal to generate the missing even-numbered harmonics. We choose $C = 25$ nF and $R = 327\ \Omega$ so that the high-pass filter's cutoff frequency is ∼20 kHz and use square-wave fundamental frequencies in the range 4-10 kHz. We amplify the harmonically-rich signal with an E&I 1140LA broadband power amplifier before sending it to the diagnostic's antenna. We measure the antenna's voltage and current for an input 4 kHz square wave signal to present in Fig. 5 the corresponding estimates of the autopower spectra. The comb structure of the signal is clear, with numerous harmonics present at similar power levels.

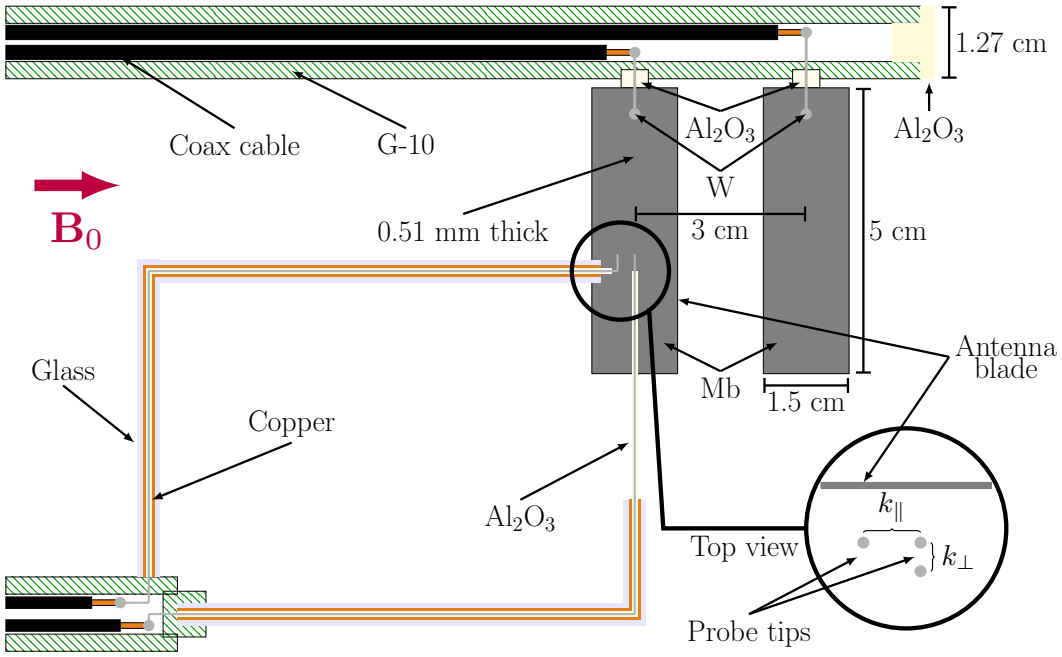

Figure 2. Antenna and receiver probes. The bottom probe arm has two probe tips that measure the wavenumber in the direction perpendicular to the plane of the antenna blades, which in our experiment corresponds to $k_\perp$. The upper probe arm has only one probe tip, which in combination with one of the other two probes (see inset top view) measures the wavenumber in the direction parallel to the axis of the G-10 tubes, which in our experiment corresponds to $k_\parallel$

.

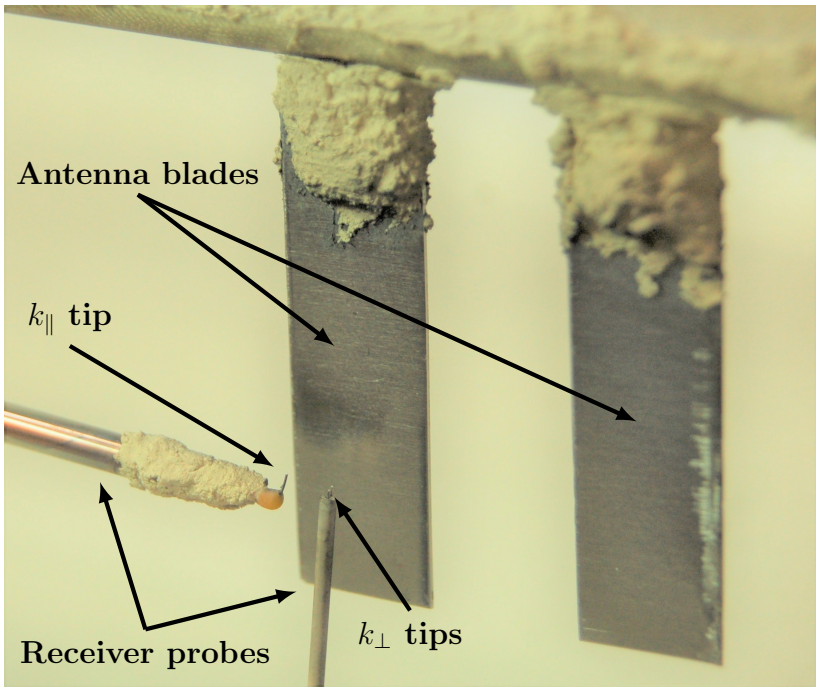

Figure 3. AWPI diagnostic. All wiring going to the antenna and probe tips runs through G-10 tubes to protect it against the plasma environment. Zirconia paste coats interfaces between wires and housing to prevent damage.

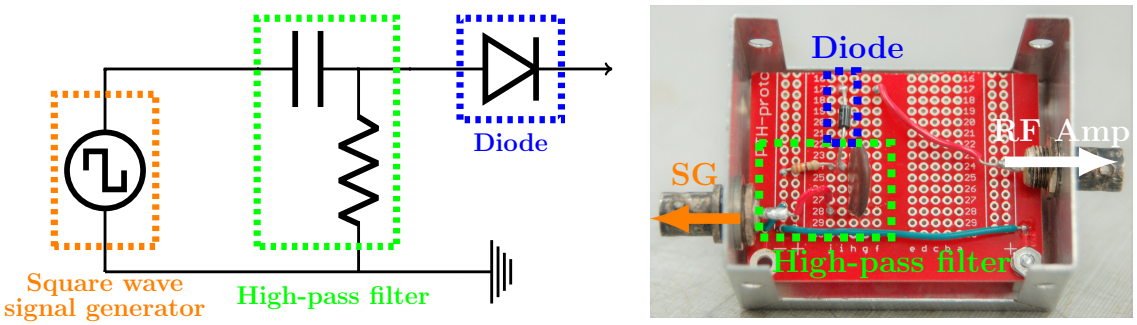

(a) Schematic (b) Hardware

Figure 4. Harmonic comb generating circuit. The high-pass fliter and diode are passive but the oscillator is a signal generator capable of outputing square waveforms. Based on the design in Ref. 21.

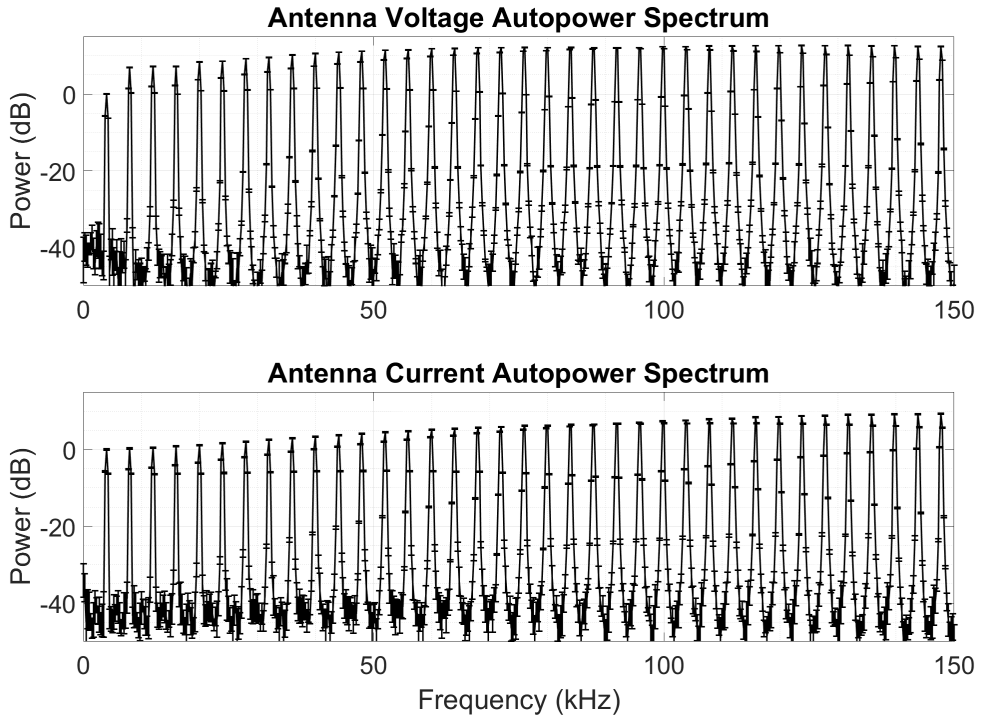

;

Figure 5. Antenna voltage and current autopower spectra. We use the power of each signal at the fundamental frequency of 4 kHz as the reference for the decibel normalization.

C. Plasma Source

We implement the AWPI diagnostic in the magnetized RF argon plasma source pictured in Fig. 6. The electron density, electron temperature, ion temperature, and background magnetic field profiles of the source have been characterized.[22] The vacuum vessel is a 132 cm long, 16.5 cm inner diameter quartz tube housed inside a 122 cm long, 10 ring solenoid. A water cooled 19.1 cm outer diameter, 22 cm long saddle antenna surrounds the quartz tube at one end of the vessel. A 1.25 kW RF source which operates at 13.56 MHz powers the saddle antenna while an L network with two Jenning 1000 pF 3 kV variable vacuum capacitors matches the RF signal to the argon plasma (VSWR in the range 1.2–1.5). At the other end of the vessel, an aluminum cross connects the quartz tube to a 140 l/s turbomolecular pump which is backed with a roughing pump. The solenoid comprises two klystron Varian 1955A magnets placed end to end, which generate an

axial background magnetic field. Table 1 presents representative values of plasma parameters at the location where we measure the dispersion relation, while Table 2 presents the source's operational parameters during the measurements.

Table 1. Representative Plasma Parameters for Plasma Source

Parameter	Value	Parameter	Value
Electron Density (n_e)	2.5×10^{17} m^{-3}	Ion Plasma Frequency ($f_{p,\mathrm{i}}$)	17 MHz
Electron Temperature (T_e)	3.5 eV	Ion Sound Speed (c_S)	3.2 km/s
Ion Temperature (T_i)	0.25 eV	Ion Thermal Velocity ($v_{th,\mathrm{i}}$)	780 m/s
Ion Larmor radius (ρ_i)	6 mm	Ion Cyclotron Frequency ($f_{c,\mathrm{i}}$)	20 kHz

Table 2. Plasma Source Operational Parameters

Parameter	Value	Parameter	Value
RF Power (P_{RF})	250 W	RF Frequency (f_{RF})	13.56 MHz
Background Magnetic Field (B_0)	526 G	Neutral Pressure (P_o)	0.1 mTorr

IV. Electrostatic Ion-Cyclotron Wave Theory

For electrostatic waves in an isothermal ($T_\perp = T_\parallel$) magnetized plasma Eq. 1 takes the form[23]

$$\mathcal{D}(\omega,\mathbf{k}) = k_\parallel^2 + k_\perp^2 + \sum_\mathrm{s} \lambda_{D,\mathrm{s}}^{-2}\left[1+\sum_n e^{-b_\mathrm{s}} I_n(b_\mathrm{s}) Z\left(\zeta_{n,\mathrm{s}}\right)\zeta_0\right] = 0, \tag{10}$$

where I_n is the n^{th} order modified Bessel function of the first kind, Z the plasma dispersion function of Fried and Conte,

$$\zeta_{n,\mathrm{s}} = \frac{\omega - n\,\omega_{c,\mathrm{s}} - k_\parallel v_{d,\mathrm{s}}}{\sqrt{2}\,k_\parallel v_{th,\mathrm{s}}}, \quad b_\mathrm{s} = \frac{k_\perp^2 v_{th,\mathrm{s}}^2}{\omega_{c,\mathrm{s}}^2}, \tag{11}$$

$\lambda_{D,\mathrm{s}}$ the species Debye length, $v_{th,\mathrm{s}}$ the species thermal velocity, $v_{d,\mathrm{s}}$ the species parallel drift velocity, and $\omega_{c,\mathrm{s}}$ the species cyclotron frequency. If we consider low-frequency oscillations ($\omega \ll \omega_{c,\mathrm{e}}$) and fully magnetized electrons ($b_\mathrm{e} \propto \rho_\mathrm{e}^2/\lambda_\perp^2 \ll 1$), we can re-express the above as[15,17]

$$k_\parallel^2 + \frac{\omega_{p,\mathrm{e}}^2}{v_{th,\mathrm{e}}^2}\left[1+\frac{\omega}{\sqrt{2}k_\parallel v_{th,\mathrm{e}}}Z(\zeta_{0,\mathrm{e}})\right] + k_\perp^2\left[1+\frac{\omega_{p,\mathrm{e}}^2}{\omega_{c,\mathrm{e}}^2}+\frac{\omega_{p,\mathrm{i}}^2\,e^{-b_\mathrm{i}}}{k_\parallel\,v_{th,\mathrm{i}}\,\omega\,b_\mathrm{i}}\sum_n n^2 I_n(b_\mathrm{i})Z(\zeta_{n,\mathrm{i}})\right] = 0. \tag{12}$$

Note that this dispersion relation has the symmetry $\omega(k_\perp) = \omega(-k_\perp)$.

Two wave modes arise as solutions to Eq. 12 in the low-frequency range ($\omega \gtrsim \omega_{c,\mathrm{i}}$) we consider: the electrostatic ion cyclotron (EIC) wave[14,24,25] and the neutralized ion Bernstein (NIB) wave.[15,26] The EIC branch exhibits the acoustic-like relation (which comes from either simplifying Eq. 12 by assuming $b_i \ll 1$ or from a simpler warm plasma fluid model[23])

$$\omega^2 = \omega_{c,\mathrm{i}}^2 + k_\perp^2 c_S^2, \tag{13}$$

where $c_S = \sqrt{T_\mathrm{e}/m_\mathrm{i}}$ is the ion acoustic speed. The NIB branch has one solution for each interval $n\,\omega_{c,\mathrm{i}} \le \omega \le (n+1)\,\omega_{c,\mathrm{i}}$, $n \ge 1$, which asymptotes to $n\,\omega_{c,\mathrm{i}}$ as $k \to \infty$. At our low-temperature plasma's operating background neutral pressure range of 0.1–1 mTorr, ion-neutral charge-exchange collisions cause the NIB wave modes to be highly damped,[27] so we expect to primarily excite EIC wave modes. The excitation of these modes requires in addition that[15]

$$\omega_{c,\mathrm{i}} < \omega_{p,\mathrm{i}}, \quad T_\mathrm{i} \lesssim T_\mathrm{e}, \quad \text{and} \quad \sqrt{2}v_{th,\mathrm{i}} \ll {}^{\omega}/_{k_\parallel} \ll \sqrt{2}v_{th,\mathrm{e}}, \tag{14}$$

which are satisfied in our experiment.

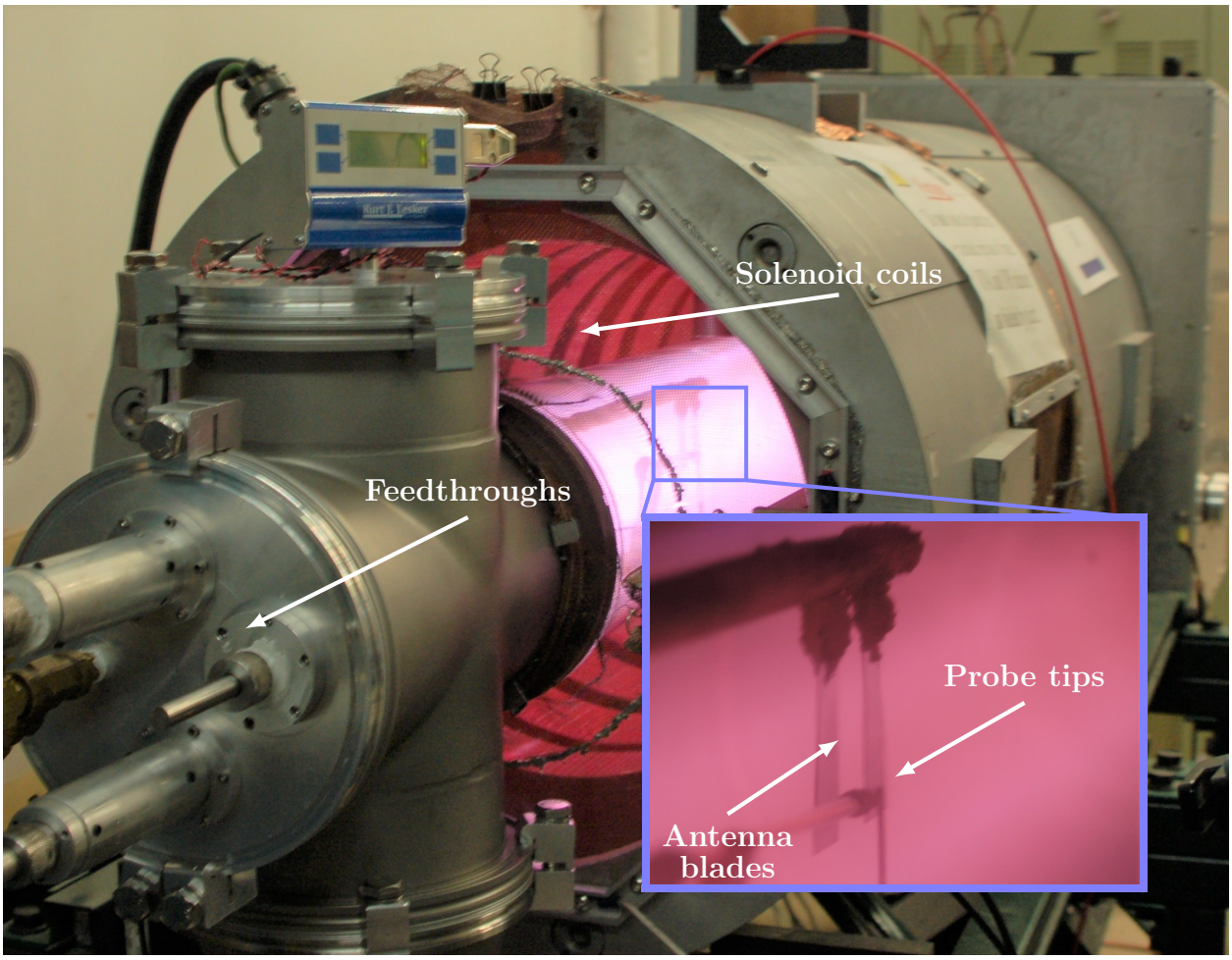

Figure 6. Argon plasma source. The saddle antenna sustains the 13.56 MHz argon discharge inside the quartz vessel. Feedthroughs in the aluminum cross provide physical access to the plasma. The antenna and receiver probes are near the center of the discharge.

V. Results and Discussion

Fig. 7 presents the estimates of the autopower and coherence spectra of the two receiver probes that take measurements in the direction perpendicular to the antenna blades. The harmonic comb structure is present in these spectra as well and the measurements at the harmonics of the fundamental frequency have high coherence with low error, satisfying our criteria for coherent wave propagation. However, to determine which wavemode has carried the signal from antenna to probes, we look at the resulting dispersion relation measurement.

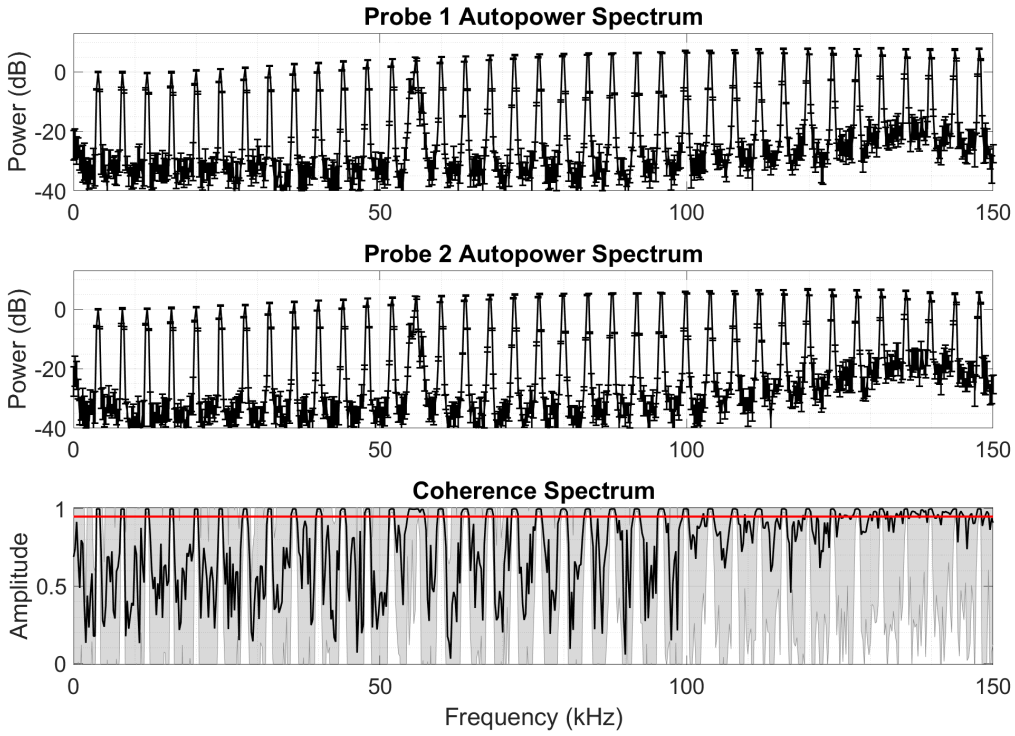

;

Figure 7. Probe signals autopower spectra. We use the power of each signal at the fundamental frequency of 4 kHz as the reference for the decibel normalization. The shaded region in the lower plot indicates the error in the coherence measurements. The red line is at a coherence of 0.95.

We present in Fig. 8 the measured real part of the dispersion relation alongside solutions to the fluid dispersion relation of EIC waves from Eq. 13 for varying electron temperatures. The data begins to deviate away from the expected dispersion relation at around 6 cyclotron harmonics (120 kHz), possibly due to diminished coupling between the antenna and electrostatic modes in the plasma. Fig. 9 displays corresponding measurements of the imaginary part of the dispersion relation. The positive imaginary wavenumbers indicate decaying waves as their amplitude is proportional to $\exp(i\mathbf{k}\cdot\mathbf{x})$. We do not have corresponding measurements of $k_{\|}$, so comparison of the measured decay to predictions of Eq. 12 is not possible. However, we compared both dispersion and decay measurements to those taken with purely sinusoidal excitations and found them to agree, upholding the claim that the AWPI technique is an expedited version of dispersion relation measurement through active wave injection.

While these results represent an encouraging demostration of a proof-of-concept experiment for the AWPI technique, we have encountered limited repeatability with the excitation of electrostatic modes. More often than not, for experimental reasons yet to be determined, the measured dispersion relation leads either to (1) $\omega/k = c$, which implies that the probes are AC coupled, or (2) $\omega/k \gg c_S$ with $\omega(k_\perp) \neq \omega(-k_\perp)$, indicating no excitation of electrostatic modes. Both cases indicate that no electrostatic modes were detected. However, in all cases where electrostatic modes were detected, the measurements were consistent with EIC wave modes and resemble the data of Figs. 8 and 9.

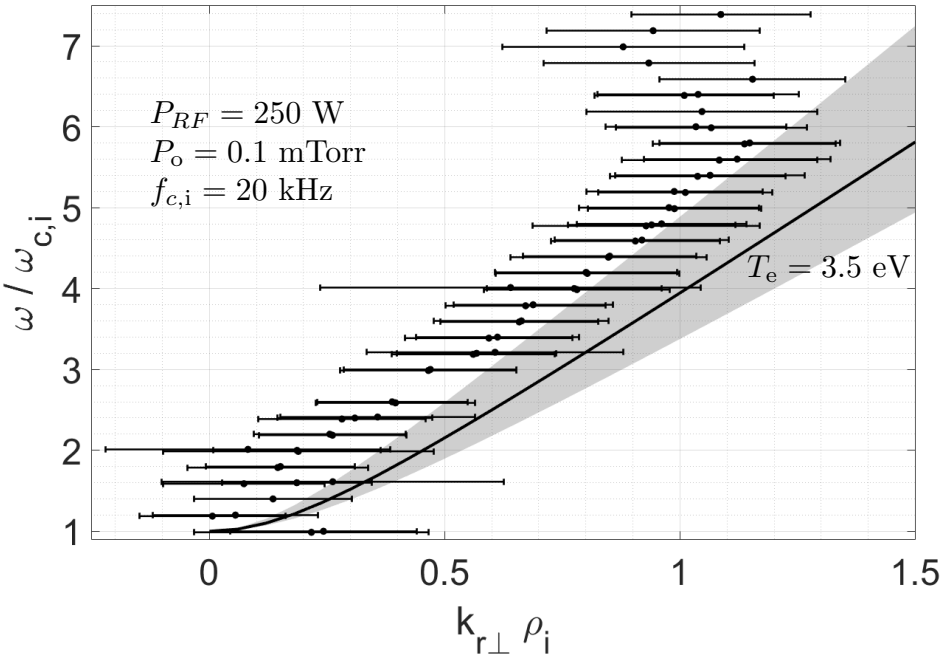

Figure 8. Measured dispersion. The gray region represents the theoretical predictions of the fluid plasma model from Eq. 13 for T_e = 2.5–5.5 eV and B_0 = 526 G. All measurements have $|\gamma_{12}| > 0.95$ with an error less than 0.05.

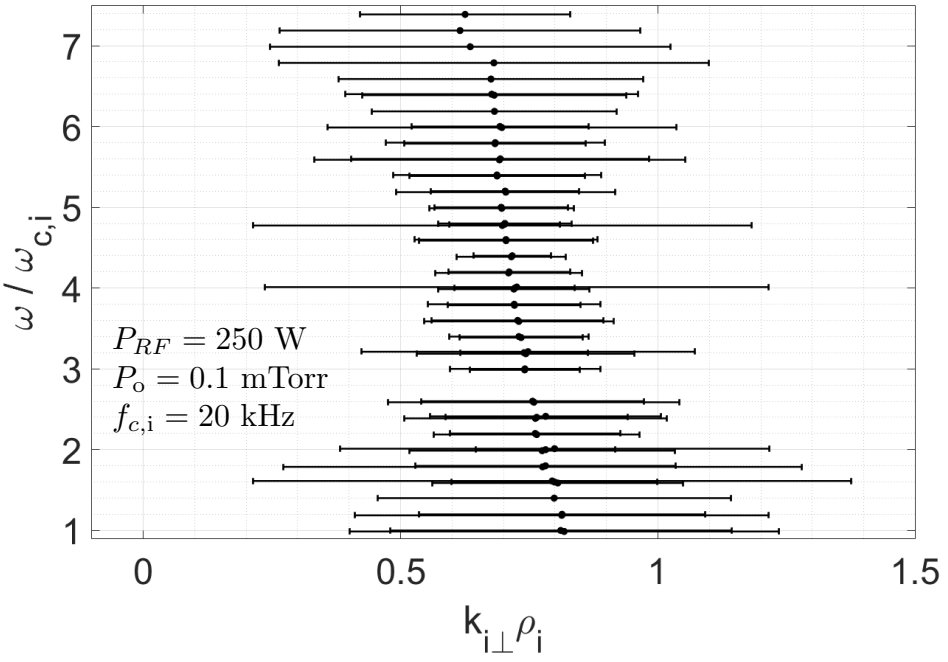

Figure 9. Measured spatial decay. All measurements have $|\gamma_{12}| > 0.95$ with an error less than 0.05.

VI. Conclusion

We presented an active wave packet injection technique for conducting expedited measurements of the dispersion relation in a plasma. The AWPI technique emits and receives harmonically-rich wave packets, measuring the linear dispersion relation simultaneously at multiple frequencies. We conducted a proof-of-concept experimental investigation of electrostatic ion-cyclotron waves in a magnetized RF argon plasma source to verify an AWPI diagnostic against fluid theory predictions of the dispersion relation. The implemented harmonic comb generating circuit outputs tens of harmonics of an input square wave's fundamental frequency. In all cases for which we detected electrostatic waves, the measured dispersion relation agreed with the fluid theory predictions for EIC waves over a span of 3–6 ion-cyclotron harmonics. Future work will characterize the extent probe pertubation affects the measurements by comparing to LIF dispersion relation measurements.

A. Electrical Diagram

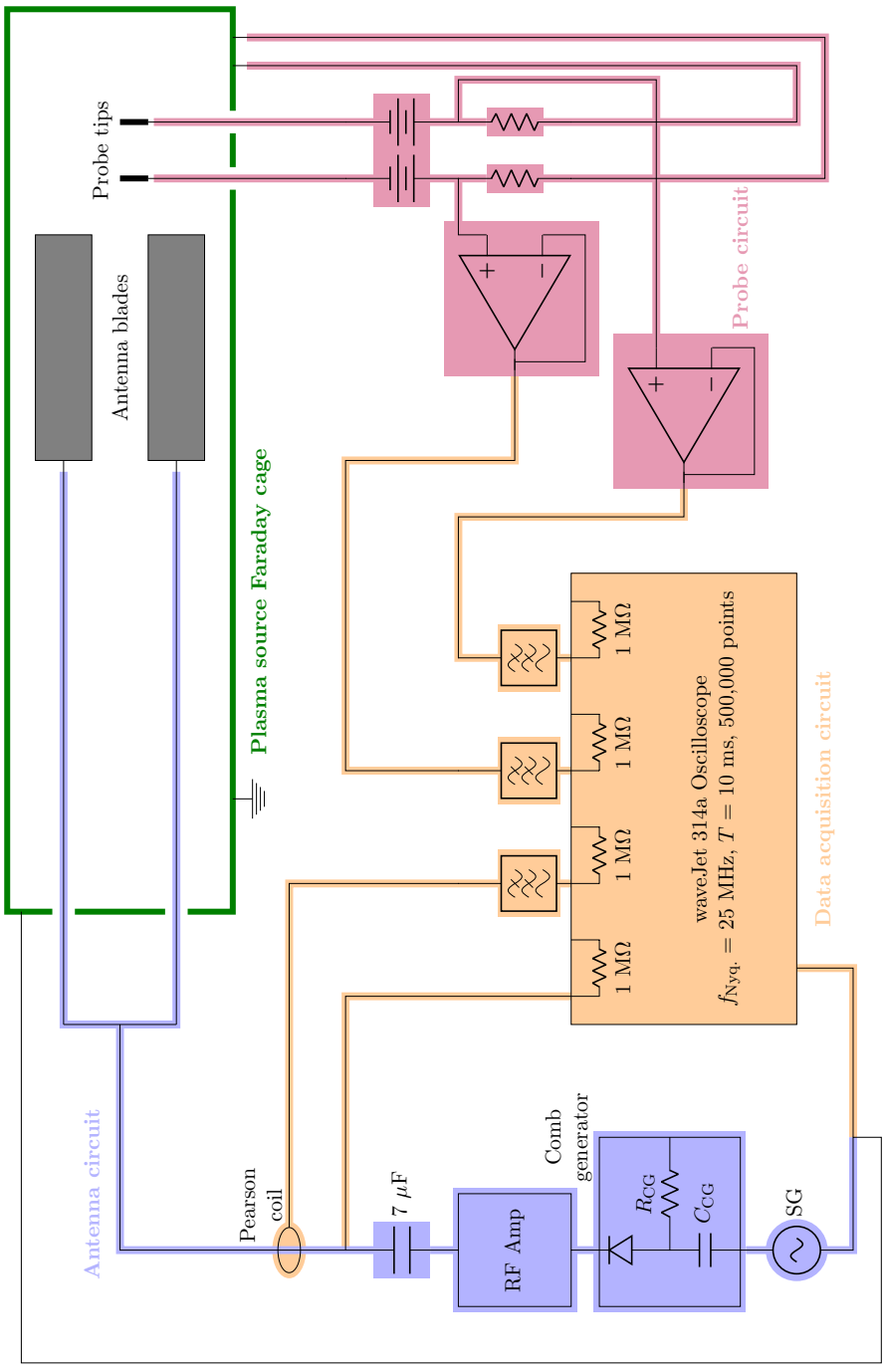

Figure 10. Electrical circuit of the experiment. The shaded regions represent the shielding of the various circuits and their connections.

References

[1]Héron, A. and Adam, J. C., "Anomalous conductivity in Hall thrusters: Effects of the non-linear coupling of the electron-cyclotron drift instability with secondary electron emission of the walls," *Physics of Plasmas*, Vol. 20, No. 8, 2013, pp. 82313.

[2]Yoshikawa, S. and Rose, D. J., "Anomalous Diffusion of a Plasma across a Magnetic Field," *Physics of Fluids*, Vol. 5, No. May 2015, 1962, pp. 334.

[3]Cappelli, M. A., Meezan, N. B., and Gascon, N., "Transport physics in Hall plasma thrusters," *40th AIAA Aerospace Sciences Meeting and Exhibit*, No. January, Reno, NV, 2002, pp. AIAA–2002–485.

[4]Jorns, B. A., Mikellides, I. G., and Goebel, D. M., "Ion acoustic turbulence in a 100-A LaB_6 hollow cathode," *Physical Review E*, Vol. 90, No. 6, 2014, pp. 063106.

[5]Choueiri, E. Y., "Plasma Oscillations in Hall Thrusters," *Physics of Plasmas*, Vol. 8, No. 4, 2001, pp. 1411–1426.

[6]Jorns, B. A. and Hofer, R. R., "Plasma oscillations in a 6-kW magnetically shielded Hall thruster," *Physics of Plasmas*, Vol. 21, No. 5, 2014.

[7]Liewer, P. C. and Krall, N. A., "Self-consistent approach to anomalous resistivity applied to theta pinch experiments," *The Physics of Fluids*, Vol. 16, No. 11, 1973.

[8]Rosenberg, M., Krall, N. A., and McBride, J. B., "Wave-induced plasma transport in the magnetic drift frequency range," *Physics of Fluids*, Vol. 28, No. 2, 1985, pp. 538.

[9]Rojas Mata, S., Choueiri, E. Y., Jorns, B., and Spektor, R., "PRINCE: A Software Tool for Characterizing Waves and Instabilities in Plasma Thrusters," *52nd AIAA/SAE/ASEE Joint Propulsion Conference*, Salt Lake City, UT, 2016.

[10]Smith, D. E., Powers, E. J., and Caldwell, G. S., "Fast-Fourier-transform spectral-analysis techniques as a plasma fluctuation diagnostic tool," *IEEE Transactions on Plasma Science*, Vol. 2, No. 4, 1974, pp. 261–272.

[11]Sarfaty, M., De Souza-Machado, S., and Skiff, F., "Direct determination of ion wave fields in a hot magnetized and weakly collisional plasma," *Physics of Plasmas*, Vol. 3, No. 12, 1996, pp. 4316–4324.

[12]Kline, J. L., Franck, C., and Spangler, R., "First order perturbed velocity distribution theory and measurement," Tech. rep., West Virginia University, 2000.

[13]Beall, J. M., Kim, Y. C., and Powers, E. J., "Estimation of wavenumber and frequency spectra using fixed probe pairs," *Journal of Applied Physics*, Vol. 53, No. 6, 1982, pp. 3933–3940.

[14]Ohnuma, T., Miyake, S., Sato, T., and Watari, T., "Propagation of Electrostatic ion Waves Near Ion Cyclotron Harmonics," *Physical Review Letters*, Vol. 26, No. 10, 1970, pp. 541.

[15]Goree, J., Ono, M., and Wong, K. L., "Observation of the backward electrostatic ion-cyclotron wave," *Physics of Fluids*, Vol. 28, No. 9, 1985.

[16]Skiff, F. and Anderegg, F., "Direct Observation of Plasma Dielectric Motion," *Physical Review Letters*, Vol. 59, No. 8, 1987, pp. 896–899.

[17]Spektor, R. and Choueiri, E. Y., "Excitation and propagation of Electrostatic Ion Cyclotron waves in rf-sustained plasmas of interest to propulsion research," *40th AIAA/ASME/SAE/ASEE Joint Propulsion Conference and Exhibit*, Fort Lauderdale, FL, 2004.

[18]Welch, P. D., "The Use of Fast Fourier Transform for the Estimation of Power SPectra: A Method Based on Time Averaging Over Short, Modified Periodograms," *IEEE Transactions on Audio and Electroacoustics*, Vol. 15, No. 2, 1967, pp. 2077.

[19]Stoica, P. and Moses, R., *Spectral Analysis of Signals*, Prentice Hall, Inc., Upper Saddle River, 2009.

[20]Brandt, A., *Noise and Vibration Analysis: Signal Analysis and Experimental Procedures*, John Wiley & Sons, Inc., UK, 2011.

[21]Kolodziej, K. E., "Comb generator design for SWaP-constrained applications," *IEEE Radio and Wireless Symposium, RWS*, Vol. 2016-March, No. 1, 2016, pp. 200–203.

[22]Jorns, B., *Experimental Characterization of Plasma Heating with Beating Electrostatic Waves*, Ph.D. thesis, Princeton University, 2012.

[23]Stix, T. H., *Waves in Plasmas*, Springer, New York, 1992.

[24]Hirose, A., Alexeff, I., and Jones, W. D., "Dispersion Measurements of Electrostatic Ion Waves in a Uniform Magnetic Field," *Physics of Fluids*, Vol. 13, No. 8, 1970, pp. 2039.

[25]Ault, E. R. and Ikezi, H., "Propagation of Ion Cyclotron Harmonic Wave," *Physics of Fluids*, Vol. 13, No. 11, 1970, pp. 2874.

[26]Lominadze, D. G. and Stepanov, K. N., "Induction of Low-Frequency Longitudinal Oscillations in a Plasma Contained in a Magnetic Field," *Sov. Phys. Tech. Phys.*, Vol. 9, 1965, pp. 1408.

[27]Spektor, R. and Choueiri, E. Y., "Measurements of Ion Energization by a Pair of Beating Electrostatic Ion Cyclotron Waves," *International Electric Propulsion Conference 2005*, 2005, pp. 1–11.